Journal of Applied Crystallography, Volume 47, Part 2, April 2014, pp. 488-494
DOI:10.1107/S1600576714000314

Energy dispersive X-ray diffraction mapping on a bench top X-ray fluorescence system

D.W. Lane[1], A. Nyombi[2], J. Shackel

Cranfield Forensic Institute, Cranfield University, Shrivenham, Swindon, SN6 8LA, UK.

Abstract

A method for energy dispersive X-ray diffraction mapping is presented using a conventional low power bench top X-ray fluorescence spectrometer, the Seiko Instruments SEA6000VX. Hyper spectral X-ray maps with a 10 µm step size were collected from polished metal surfaces, sectioned Bi, Pb and steel shot gun pellets. Candidate diffraction lines were identified by eliminating those that matched a characteristic line for an element and those predicted for escape peaks, sum peaks and Rayleigh and Compton scattered primary X-rays. The maps showed that the crystallites in the Bi pellet were larger than those observed in the Pb and steel pellets. The application of bench top spectrometers to energy dispersive X-ray diffraction mapping is discussed.

Keywords

X-ray fluorescence, X-ray diffraction, energy dispersive X-ray diffraction, mapping, texture, shot gun pellet, forensic

1: Corresponding author, email D.W.Lane@cranfield.ac.uk, telephone +44(0)1793 785226

2: Permanent address: Directorate of Government Analytical Laboratory, Plot 2 Loudel Road, P.O. Box 2174, Kampala, Uganda.

Introduction

X-ray fluorescence spectroscopy (XRF) is one of the most common non-destructive techniques for the elemental analysis of materials and is routinely used to examine specimens in a diverse range of fields such as environmental and forensic science, archaeology, electronics and metallurgy.

In a conventional bench top XRF spectrometer a collimated primary X-ray beam is directed at the analytical specimen's surface. This causes characteristic X-rays to be generated by fluorescence, which are then collected by a detector located close by. The energy and intensity of the characteristic X-rays are used to identify and quantify the elements in the specimen. However, the X-ray spectrum will also include additional features that can complicate analysis such as Rayleigh and Compton scattered primary X-rays, escape peaks and sum peaks. These artefacts are relatively easy to predict and can usually be accommodated. However, in the case of highly crystalline specimens the enhanced reflection of the primary X-rays by diffraction can result in additional artefact peaks that are more difficult to predict and are quite often neglected in introductory texts on the subject.

If the measurement geometry in a spectrometer (figure 1 a) is considered along with Bragg's law the conditions for diffraction are satisfied by,

$$\frac{h.c}{E_\theta} = \lambda_\theta = 2d.sin\left(\frac{\theta}{2}\right) \quad (1)$$

Where λ_θ and E_θ are the wavelength and energy required for the incident X-rays to diffract from a crystal lattice spacing *d* at a scattering angle θ; *h* is Plank's constant and *c* is the speed of light. In an XRF spectrometer the experimental arrangement can be considered to be the reverse of that found in a conventional X-ray diffractometer that operates with a fixed λ_θ and a variable θ; whereas in the spectrometer the experimental geometry (i.e. θ) is fixed and E_θ and hence λ_θ is varied through the use of a polychromatic primary X-ray beam. Consequently, when a polycrystalline specimen is examined by XRF some of its crystallites will be aligned such that the normal to their lattice planes bisect the supplement of scattering angle and diffraction occurs, creating a peak on the X-ray spectrum at the corresponding E_θ with a width governed by the collimation of the primary beam and the detector's solid angle. While this peak would normally be considered a spectral artefact it can be used to gain information about the structure of the specimen. Indeed, energy dispersive X-ray diffraction (EDXRD) at a fixed angle is often used to examine materials in special applications. The high X-ray flux available from synchrotrons is used for transmission EDXRD [1, 2, 3] with the forward scattering geometry resulting in diffraction peaks at energies above those for the characteristic emission lines. This arrangement is particularly suited to applications where access to the specimen is limited as in high temperature or high pressure measurements [4, 5, 6, 7, 8]. Transmission EDXRD has also been used for security applications, such as detecting drugs and explosives, including both crystalline solids and liquids [9, 10, 11, 12, 13]. For some laboratory scale instruments the back scatter geometry has been adopted. Sun et al [14] used polycapillary optics to collimate of both incident and diffracted X-ray beams, and several portable instruments have been developed for archaeological applications [15, 16, 17], some of which have also been used for simultaneous XRF. In these cases the back scatter geometry and portability were demanded by the practical limitation of only being able analyse from one side and not being able to move artefacts into the laboratory. Imafuku [18] constructed a laboratory scale instrument to map steel sheet, using a 12 kW rotating anode X-ray source with a Ge detector positioned in a forward scattering direction.

Published by International Union of Crystallography. This is the Author Accepted Manuscript issued with:
Creative Commons Attribution Non-Commercial License (CC:BY:NC 4.0).
The final published version (version of record) is available online at DOI:10.1107/S1600576714000314. Please refer to any applicable publisher terms of use.

This collected a full X-ray spectrum at each location, taking about 5.5 hours to map a 25 by 24.5 mm area. In this paper we present some results from a commercial bench top XRF spectrometer with a 50 W X-ray source that was used for EDXRD mapping from different metals. This opens up new potential applications for small low powered laboratory instruments.

Experimental method

The analytical specimens used to test the EDXRD mapping process consisted of three shot gun pellets that had been mounted in resin and polished using 1 μm diamond paste to reveal their inner structure. The pellets were commercially sourced and made from alloys of Bi, Pb and Fe, and were approximately 2.5 mm in diameter. The X-ray spectroscopy measurements were undertaken on a Seiko Instruments SEA6000VX bench top XRF spectrometer with a Rh X-ray tube operating at a potential of 50 kV and with a current of 1000 μA. The primary beam was collimated to a width of 0.2 mm and the spectrometer's energy dispersive Vortex Si semiconductor detector was positioned at θ = 135°. Spectral maps were collected using the instrument's 'Mapping Station' software and a step size (i.e. pixel width) of 10 μm and a data collection time of 0.5 s at each data collection point. This resulted in mapping times of around 10 hours. The diffraction lines were identified in the resulting maps by plotting the total spectrum collected over selected areas and using a process of elimination on the observed lines, eliminating those that matched a characteristic line for an element, provided that the other lines for the element could be accounted for, and those predicted for escape peaks, sum peaks and Rayleigh and Compton scattered primary X-rays.

Results

Figure 2 presents the X-ray spectra collected from large areas (around 4 mm^2) of the polished pellet cross sections. The most prominent features of the spectra can be seen to be the characteristic M and L lines for the Bi and Pb pellets and the characteristic K lines for Fe and Mn for the steel pellet. The spectrum from the steel pellet also has some sum peaks caused by the high intensity Fe lines and some small Rh L lines caused by Rayleigh scatter from the X-ray tube in the spectrometer. These lines are most probably hidden by the M lines in the spectra for the Bi and Pb specimens, which respectively contain traces of Sn and Sb which are elements that are frequently added to shot gun pellets to affect their manufacturing and mechanical properties. In addition, each spectrum has several other lines that cannot be accounted for and can be considered to be candidate diffraction lines.

X-ray maps for the characteristic lines of the major element in each pellet are presented in Figures 3 to 5 (Bi Lα, Pb Lα and Fe Kα respectively). As expected these maps confirm that the metals are very uniformly distributed across each pellet and that any variation in the intensity of their diffraction lines is unlikely to be related to changes in their concentrations. The only features visible on each of the maps is increased emission on the top edge of the pellets. This is caused by the off-axis position of the X-ray detector during data collection (see figure 1a) which results in less self-absorption of the X-rays at the top edge of the pellets as their exit path to the detector is through the low atomic number mounting resin. Maps from selected diffraction lines are included in each figure, and in each

case reveal regions of greatly increased X-ray scatter and crystallographic texture within the pellet. In the case of the Bi pellet (Figure 3) this largely comprises of two regions corresponding to increased scattering at both 4.753 keV (d-spacing 1.413 Å) and 8.159 keV (d-spacing 0.823 Å), and at 4.173 keV (d-spacing 1.609 Å). The complicated shape of these regions indicate that they may consist of collections of aligned crystallites. The crystallographic textures revealed within the Pb and steel pellets (Figures 4 and 5) are similar to each other, but quite different to that of the Bi pellet. In both cases there are fewer regions of increased X-ray scatter and they are smaller in size than for the Bi pellet. Optical micrographs for the Bi and steel pellets are presented in figure 6. This shows that the structure of the Bi pellet was indeed different to that for the steel pellet with a larger crystallite size and regions where the crystallites have the same orientation. The structure of the Pb pellet was similar to that for the steel pellet, with a smaller crystallite size than suggested by the widths of the regions observed in the X-ray maps. These may appear larger because of neighbouring crystallites having very similar orientations that are combined due to the angular resolution of the spectrometer.

Discussion

The equivalent d-spacings for the diffraction lines were calculated using equation 1 and were compared to values listed in the ICDD database [19], and the indexed lines for each specimen are summarised in Table 1. In each case the low concentrations of minor elements meant that the alloys could be represented as a single phase material, with Bi having a rhombohedral structure, Pb having a face centred cubic structure and iron having a body centred cubic structure. A linear regression to the data is presented in figure 7 which gave a coefficient of determination (R^2) of 0.999 and shows that the calibration of the system and assignment of X-ray lines was consistent across all three samples.

The X-ray maps presented in figures 3 to 5 show that a bench top spectrometer can be used to examine crystallographic texture using EDXRD. In the case of the spectrum from the Bi pellet the 4.753 and 8.159 keV reflections are very well defined (see figure 2a) and give very similar maps (see figure 3) with a large, high intensity area present at the top of the pellet. This shows that for the crystallites in this region there is a strong correlation between these two reflections, and an anti-correlation with the 4.173 keV reflection which is only apparent at the bottom of the pellet. These reflections are unlikely to be characteristic X-ray lines. The closet corresponding emission line for the 4.753 keV reflection would be the La Lα (4.651 keV), Ba Lβ (4.828 keV) or I Lγ (4.801) lines which are a poor match, and the other associated emission lines for these elements are absent. The closet corresponding emission line for the 8.159 keV reflection would be the Ta Lα line at 8.146 keV. If this line were caused by Ta its associated Lβ and Lγ lines (9.343 and 10.895 keV) would be hidden by the Bi L1 and Bi Lα lines. Therefore, if the texture apparent in the map from the 8.159 keV peak were caused by the fluorescence of Ta (not diffraction) the same texture should be present in a map of the Bi L1 line because of the underlying Ta Lβ line. This was not observed supporting the assignment of the 8.159 keV peak as a diffraction line. Similarly, the 4.173 keV reflection is coincident with the Sn Lγ line, and while this element is known to be present in the pellet, similar maps from the associated Sn Lα and Lβ lines showed no significant variation across the entire surface of the pellet, supporting the assignment of the peak as a diffraction line. These and several other reflections were

indexed and included in Table 1. The assignment of some of the lines was less certain than for the other pellets and while the peak at 8.159 keV that appears at the top of the pellet is a reasonable match to the (048) reflection it doesn't correlate with the (024) reflection which appears at the bottom of the pellet. The assignment of the (024) reflection is supported by a very small reflection from the (012) in the same area of the pellet, and it is possible that the peak at 8.159 keV is a different reflection such as the (1310), (0213) or (0114).

The X-ray spectrum from the Pb pellet (figure 2 b) was very similar to that from the Bi pellet. However the lines attributed to diffraction where not as well defined and the resulting maps (figure 4) have a very different structure with small, poorer contrast islands as opposed to large high contrast areas, suggesting a smaller crystallite size. The map for the Pb Lα line shows a very uniform signal across the whole of the pellet. However that for the Pb Mα line (2.343 keV) reveals two small higher intensity islands on its edge. These are believed to be caused by the Pb Mα line coinciding with the Pb (111) reflection, which has a d-spacing of 2.855 Å and scatters at an energy of 2.352 keV. The (200) reflection lies close-by at an energy of 2.69 keV, and shows clearer signs of diffraction with several higher contrast crystallites of similar diameter to those from the (111) reflection. The peak at 4.753 keV is believed to be the Pb (222) reflection and occurs at the same energy as the Bi (122), and is again unlikely to be a characteristic X-ray line for the same reasons as already given above.

The X-ray maps from the steel pellet (figure 5) show that its crystallite size is probably very similar to that for the Pb pellet, with the Fe Kα line showing a uniform composition and well resolved peaks at 3.351 and 4.673 keV (figure 2c). These are free from neighbouring lines that could suggest they result from fluorescence as opposed to diffraction and are believed to be the Fe (110) and (200) reflections. The situation for the Fe (211) reflection is less clear as it lies at 5.895 keV, the energy of the Kα fluorescence line for Mn which is a common component of steel. However, it is not possible to conclusively attribute this line to Mn as the position of its Kβ line clashes with the very strong Fe Kα line. However, it is very likely that the 5.895 keV line is caused at least in part by diffraction as its map shows some very clear structure with islands (crystallites) of very similar size to that seen for the (110) and (200) reflections.

The spectral range of the SEA6000VX is from 1 to 50 keV, which corresponds to a d-spacing range from 6.71 to 0.134 angstroms. However, the practical range over which diffraction measurements can be made is limited by several factors and is biased towards low energies because low index reflections tend to have a greater relative intensity than higher index reflections. In practice the position of fluorescence lines is likely to place the greatest limitation on which reflections can be resolved, and to mitigate against overlapping characteristic lines would require changing to a smaller scattering angle and either a glancing primary beam or a transmission geometry, so that the energy of the diffraction lines is greater than the characteristic line energy. This is the technique adopted by large scale facilities and is not (currently) possible for bench top spectrometers that have a limited primary beam energy and usually have a fixed detector angle. It should also be noted that the arrangement for bench top diffraction (figure 1a) doesn't follow the conventional '$\theta/2\theta$' geometry found in most laboratory diffractometers. Consequently the diffracting planes are not parallel with the sample surface and to replicate the '$\theta/2\theta$' geometry the sample would have to be tilted to and angle of $(180° - \theta)/2$, 22.5° in the present study (see figure 1b). In practice, tilting the specimen may limit its physical size because of clashing with other parts of the spectrometer.

Conclusions

The main focus of the work presented in this paper was to determine whether a commercial XRF spectrometer could be used for EDXRD and map the crystallographic texture within a material. The maps presented in Figures 3 to 5 show that this has been achieved. Structural differences in the shot gun pellets were apparent from the diffraction maps and were confirmed using optical microscopy. It is possible that this technique could be used in the forensic analysis of shot gun pellets, which is difficult as being fired from a smooth bored weapon they do not present the striation marks found on bullets. While the observed diffraction lines were of low intensity it was possible to identify which reflection they corresponded to with a good degree of certainty, and the calibration presented in figure 2 shows that this was consistent across all three specimens. The maps presented cover relatively small areas (around 10 mm^2), although the mapping stage of the spectrometer used has a range of 250 by 200 mm, and can be operated with a beam collimator width of up to 3 mm. While this presents additional functionality for the instrument its application to a wide range of samples will be governed by some important practicalities. Firstly, the low intensity of the diffraction lines demands a high X-ray tube power and a long mapping time, although in other tests reasonable maps were obtained in a shorter time by increasing the pixel size and reducing the time per pixel. In the existing system the back scatter angle limits diffraction to the low energy region of spectrum and introduces clashes with fluorescence lines. This would be a greater problem for compounds.

Acknowledgements

The authors would like to thank Professor Keith Rogers for valuable discussions on X-ray diffraction and Adrian Mustey for preparing the specimens. One of the authors (A. Nyombi) would like to thank the Netherlands Initiative for Capacity building in High Education (NICHE) for their support for this work.

References

[1] V. Honkimäki, P. Suortti, J. Synchrotron Rad., 14 (2007) 331-338.

[2] Ch. Genzel, I.A. Denks, J. Gibmeier, M. Klaus, G. Wagener, Nucl. Instr. and Meth. A, 578 (2007) 23–33.

[3] O. Lazzari, C. K. Egan, S. D. M. Jacques, T. Sochi, M. Di Michiel, R. J. Cernikcan, P. Barnes, J. Synchrotron Rad., 19 (2012) 471-477.

[4] O.F.Yagafarov, Y. Katayama, V.V. Brazhkin, A.G. Lyapin, H. Saitoh, High Pressure Research, 33 (2013) 191–195.

[5] M. J. Styles, M. R. Rowles, I. C. Madsen, K. McGregor, A. J. Urban, G. A. Snook, N. V. Y. Scarlett, D. P. Riley, J. Synchrotron Rad., 19 (2012) 39–47.

[6] Jing Liu, R.Z. Che, J. Zhao, Y.H. Jing, Y. Yang, X. Ju, Nucl. Instr. and Meth. A, 467-468 (2001) 1069-1072.

[7] W. Paszkowicz, Nucl. Instr. and Meth. B, 198 (2002) 142–182.

[8] P. Norby, Current Opinion in Colloid & Interface Science, 11 (2006) 118-125.

[9] Yu Zhong, Bai Sun, Daoyang Yu, Wei Li, Yu Zhang, Minqiang Li, Jinhuai Liu, Procedia Engineering, 7 (2010) 135–142.

[10] Lei Li, Minqiang Li, Bai Sun, Jin-huai Liu, Fang Zhang, Procedia Engineering, 7 (2010) 147–150.

[11] Wei Li, Fang Zhang, Daoyang Yu, Bai Sun, Minqiang Li, Jinhuai Liu, J. Chemometrics, 25 (2011) 631–635.

[12] Yu Zhong, Minqiang Li, Bai Sun, Jin Wang, Fang Zhang, Daoyang Yu, Yu Zhang, Jinhuai Liu, Measurement, 45 (2012) 1540–1546.

[13] C. Crespy, P. Duvauchelle, V. Kaftandjian, F. Soulez, P. Ponard, Nucl. Instr. and Meth. A, 623 (2010) 1050-1060.

[14] Tianxi Sun, Zhiguo Liu, Xunliang Ding, Nucl. Instr. and Meth. B, 262 (2007) 153-156.

[15] M. Uda, Nucl. Instr. and Meth. B 226 (2004) 75.

[16] M. Uda, A. Ishizaki, R. Satoh, K. Okada, Y. Nakajima, D. Yamashita, K. Ohashi, Y. Sakuraba, A. Shimono, D. Kojima, Nucl. Instr. and Meth. B, 239 (2005) 77–84

[17] A. Mendoza Cuevas, H. Perez Gravie, Nucl. Instr. and Meth. A, 633 (2011)72–78.

[18] M. Imafuku, Advances in X-ray Analysis, 40 (1996), 236

[19] International Centre for Diffraction Data, Newtown Square, PA, USA.

Figure and table captions

Figure 1 (a) bench top XRF geometry, (b) specimen tilted to make lattice plans parallel to surface.

Figure 2 X-ray spectra collected from sectioned metal pellets, (a) bismuth, (b) lead and (c) steel. Diffraction lines indexed as in Table 1.

Figure 3 EDXRD maps from the bismuth pellet (a) Bi Lα, (b) 4.173 keV reflection, (c) 4.753 keV reflection, (d) 8.159 keV reflection.

Figure 4 EDXRD maps from the lead pellet (a) Pb Lα, (b) Pb Mα, (c) 2.690 keV reflection, (d) 4.753 keV reflection.

Figure 5 EDXRD maps from the steel pellet (a) Fe Kα, (b) 3.351 keV reflection, (c) 4.673 keV reflection, (d) 5.895 keV reflection.

Figure 6 Optical micrographs of etched polished surfaces, (a) Bi pellet and (b) steel pellet.

Figure 7 Comparison of d-spacing for assigned lines (d_{obs}) and those published in the ICDD database (d_{ICDD}).

Table 1 Indexed EDXRD lines.

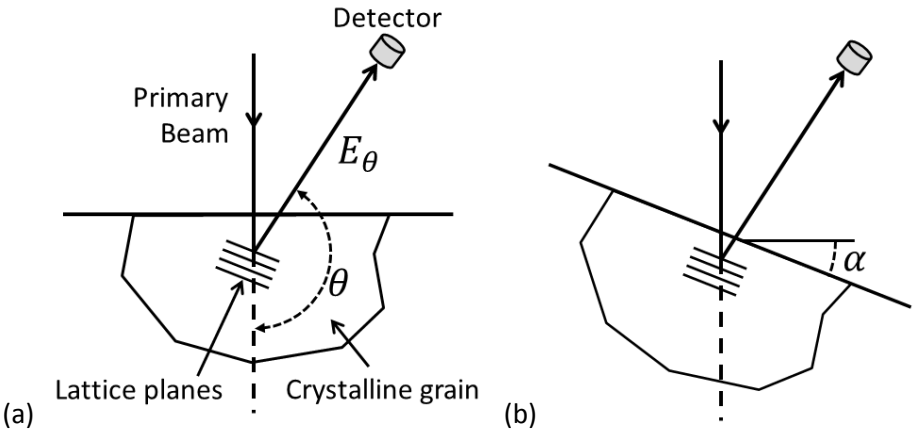

Figure 1 (a) bench top XRF geometry, (b) specimen tilted to make lattice plans parallel to surface.

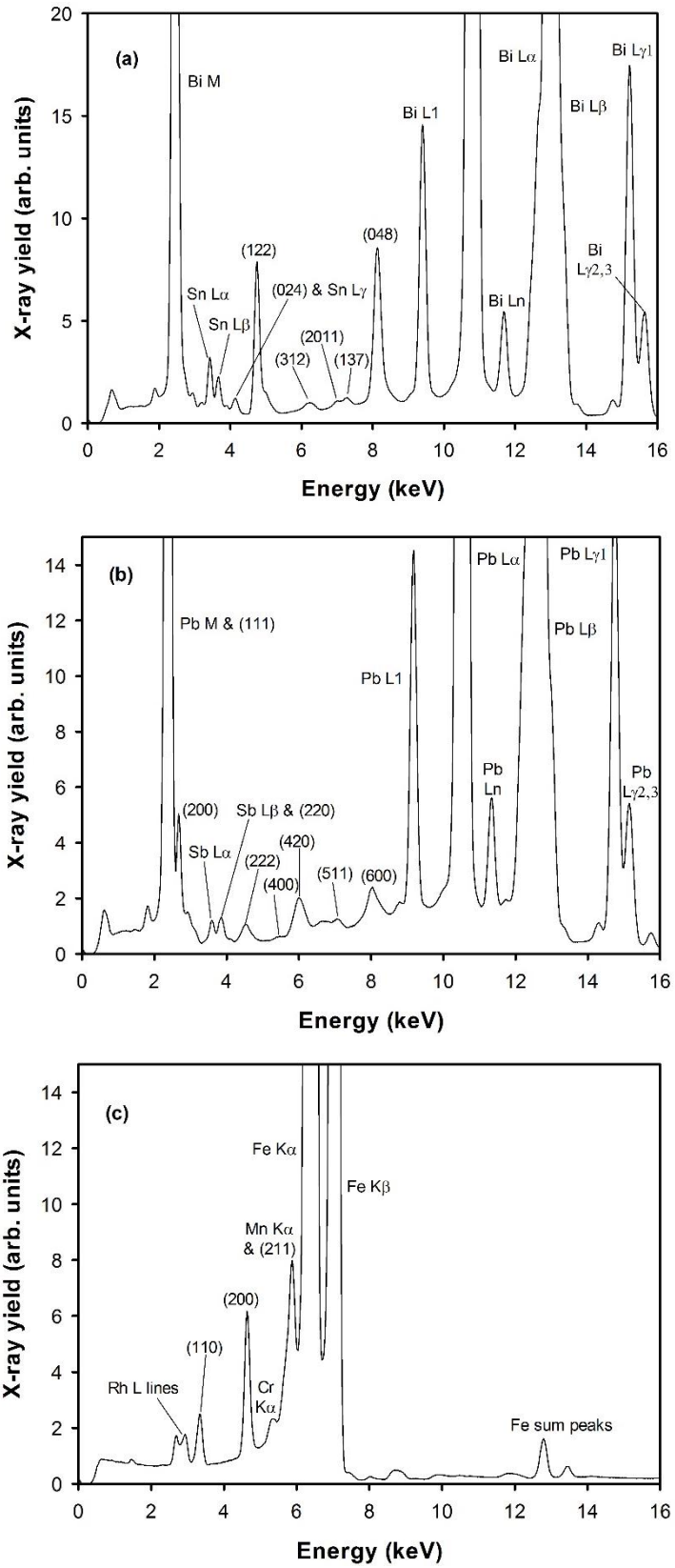

Figure 2 X-ray spectra collected from sectioned metal pellets, (a) bismuth, (b) lead and (c) steel. Diffraction lines indexed as in Table 1.

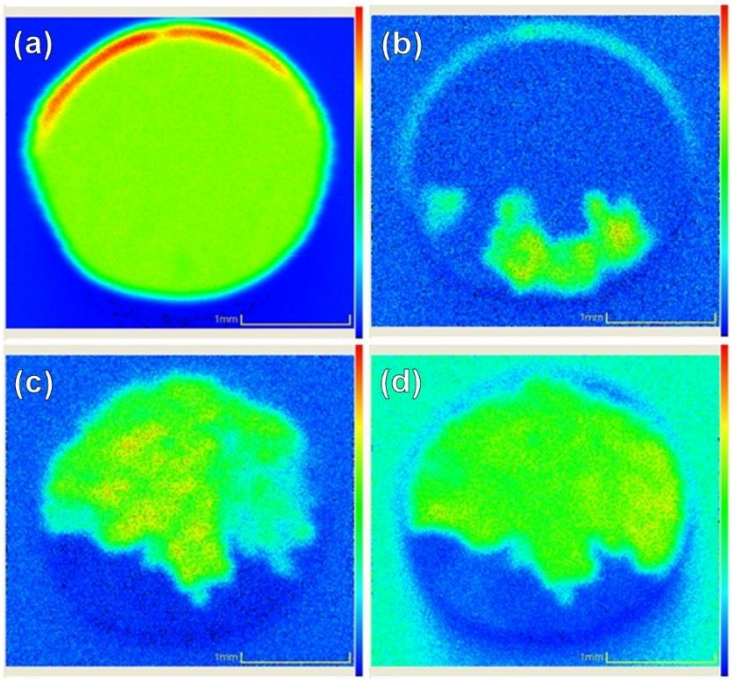

Figure 3 EDXRD maps from the bismuth pellet (a) Bi Lα, (b) 4.173 keV reflection, (c) 4.753 keV reflection, (d) 8.159 keV reflection.

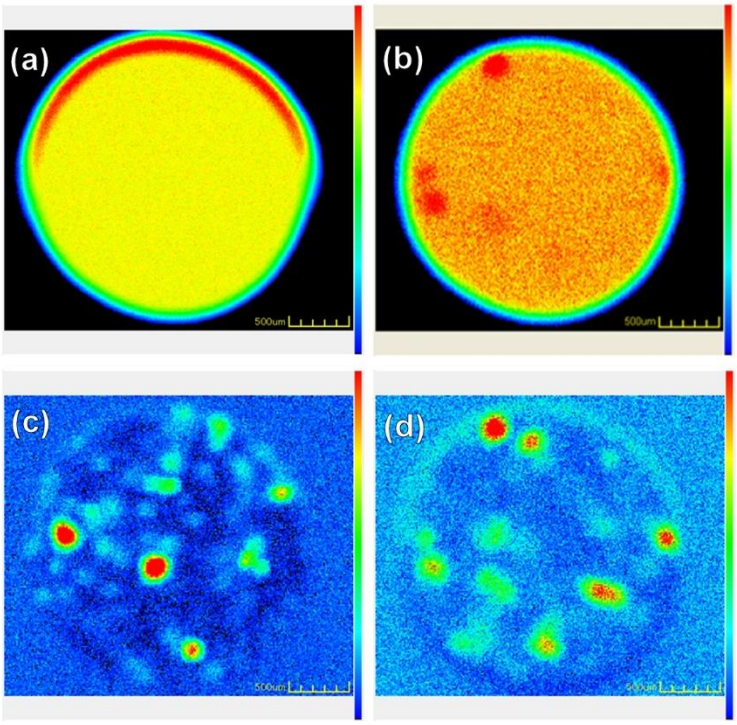

Figure 4 EDXRD maps from the lead pellet (a) Pb Lα, (b) Pb Mα, (c) 2.690 keV reflection, (d) 4.753 keV reflection.

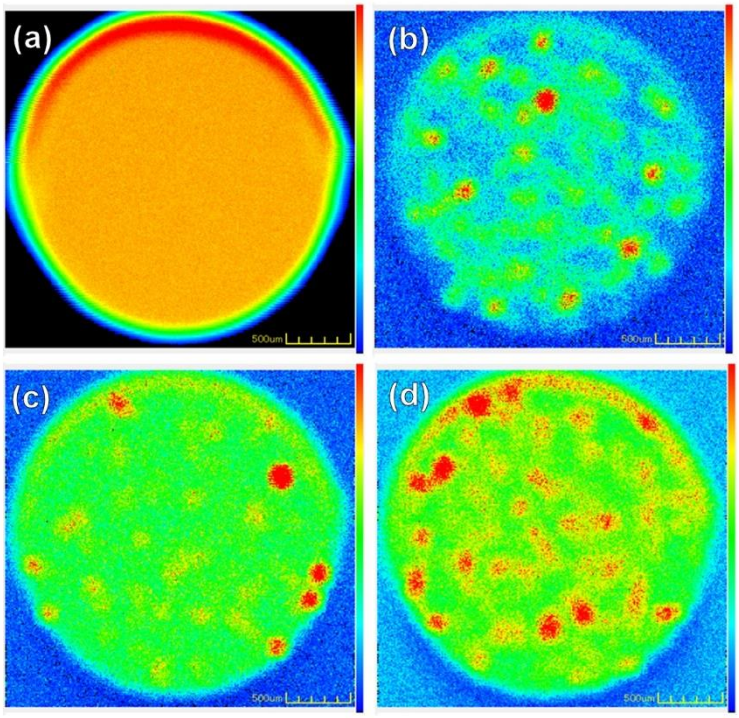

Figure 5 EDXRD maps from the steel pellet (a) Fe Kα, (b) 3.351 keV reflection, (c) 4.673 keV reflection, (d) 5.895 keV reflection.

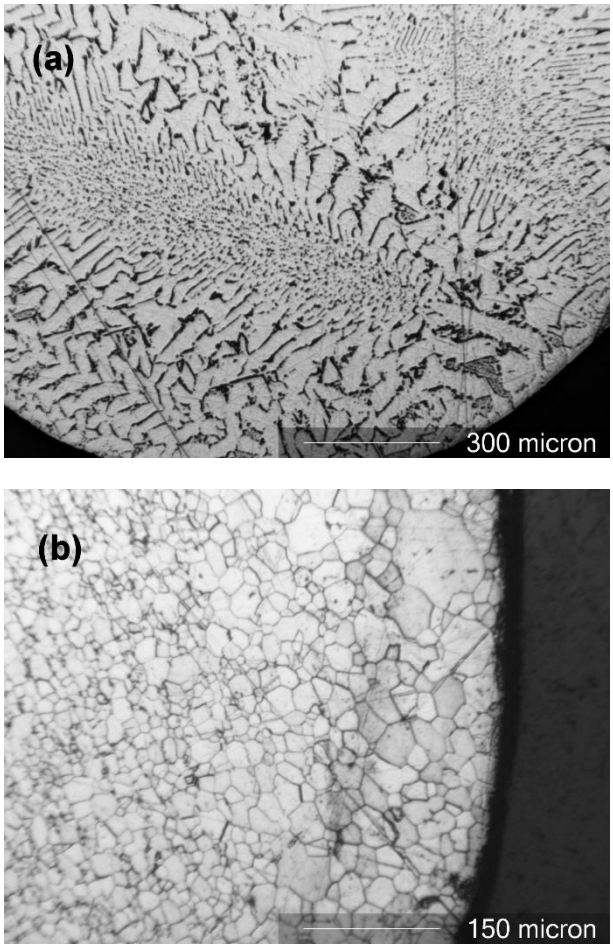

Figure 6 Optical micrographs of etched polished surfaces, (a) Bi pellet and (b) steel pellet.

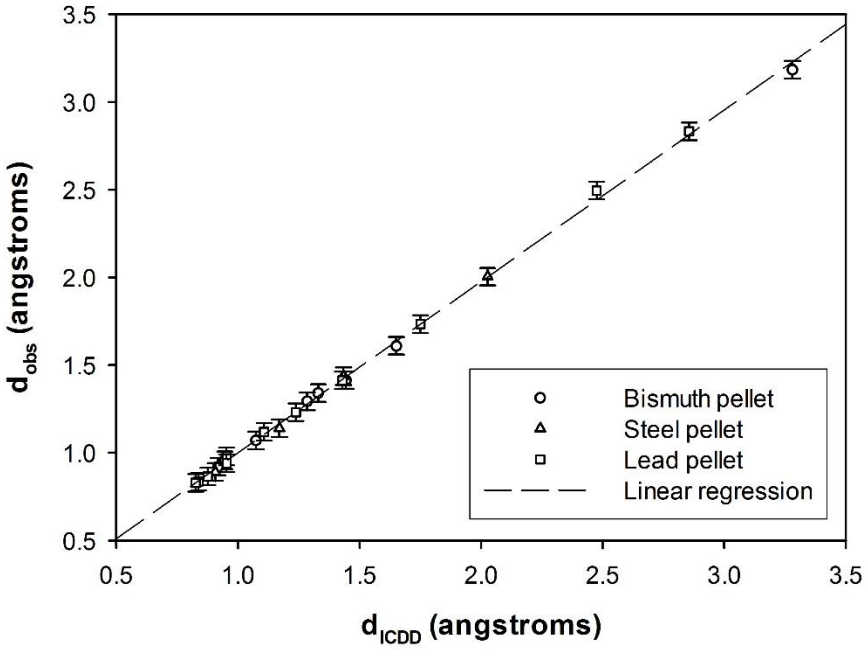

Figure 7 Comparison of d-spacing for assigned lines (d_{obs}) and those published in the ICDD database (d_{ICDD}).

Table 1 Indexed EDXRD lines.

Specimen	Peak position (keV)	d-spacing (Å)	ICDD reported value	
			d-spacing (Å)	Reflection (*hkl*)
Bismuth *(ICDD card 44-1246)*	2.109	3.184	3.28	012
	4.173	1.609	1.6505	024
	4.753	1.413	1.4436	122
	5.014	1.339	1.3303	214
	5.194	1.293	1.2843	027
	6.276	1.070	1.0741	312
	7.017	0.957	0.9458	2011
	7.297	0.920	0.918	137
	8.159	0.823	0.820	048
Lead *(ICDD card 4-686)*	2.37	2.833	2.855	111
	2.69	2.496	2.475	200
	3.872	1.734	1.750	220
	4.753	1.413	1.429	222
	5.455	1.231	1.238	400
	6.000	1.119	1.1069	420
	7.137	0.941	0.9526	511
	7.758	0.866	0.8752	440
	8.039	0.835	0.8369	531
	8.099	0.829	0.8251	600
Steel *(ICDD card 6-696)*	3.351	2.004	2.0268	110
	4.673	1.437	1.4332	200
	5.895	1.139	1.1702	211
	7.538	0.891	0.9064	310